INTERNATIONAL JOURNAL OF HYDROGEN ENERGY 47 (2022) 20973–20986

Available online at www.sciencedirect.com

ScienceDirect

journal homepage: www.elsevier.com/locate/he

Multilayer additive manufacturing of catalyst-coated membranes for polymer electrolyte membrane fuel cells by inkjet printing

Andreas Willert [a,*], Farzin Z. Tabary [b], Tatiana Zubkova [b], Paolo E. Santangelo [c,d], Marcello Romagnoli [d,e], Reinhard R. Baumann [b]

[a] Fraunhofer Institute for Electronic Nano Systems, Chemnitz, Germany
[b] Institute for Print and Media Technology, Technische Universität Chemnitz, Chemnitz, Germany
[c] Dipartimento di Scienze e Metodi Dell'Ingegneria, Università Degli Studi di Modena e Reggio Emilia, Reggio Emilia, Italy
[d] InterMech – MO.RE., Centro Interdipartimentale per La Ricerca Applicata e I Servizi Nel Settore Della Meccanica Avanzata e Della Motoristica Dell'Università Degli Studi di Modena e Reggio Emilia, Modena, Italy
[e] Dipartimento di Ingegneria "Enzo Ferrari", Università Degli Studi di Modena e Reggio Emilia, Modena, Italy

HIGHLIGHTS

- Inkjet printing of PEMFC catalytic and membrane layers was successfully performed.
- Three approaches were developed and realized towards full additive manufacturing.
- Layer thickness and Pt-loading met target values and were overall homogeneous.
- Inkjet-printed CCM proved effective in terms of electrochemical performance.
- Inkjet-printed CCM yielded peak power density 15% higher than that of baseline CCM.

GRAPHICAL ABSTRACT

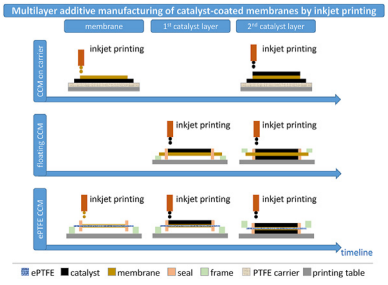

ARTICLE INFO

Article history:
Received 11 January 2022
Received in revised form
31 March 2022

ABSTRACT

Inkjet printing is a versatile, contactless and accurate material deposition technology. The present work is focused on developing innovative strategies for inkjet printing of Catalyst-Coated Membranes (CCM) by performing Additive Manufacturing (AM) applied to Polymer Electrolyte Membrane Fuel Cells (PEMFC), without resorting to intermediate substrates. Three different approaches for AM are presented and discussed: a) inkjet-printing of the

Abbreviations: AM, additive manufacturing; CCM, catalyst coated membrane; DoD, drop on demand; GDL, gas diffusion layer; MEA, membrane electrode assembly; PBI, polybenzimidazole; PEFC/PEMFC, polymer electrolyte membrane fuel cell; PTFE/ePTFE, (expanded) polytetrafluoroethylene; SEM, scanning electron microscopy; XRF, X-ray fluorescence spectroscopy.

* *Corresponding author.* Fraunhofer Institute for Electronic Nano Systems, Technologie-Campus 3, 09126, Chemnitz, Germany.
E-mail address: Andreas.Willert@enas.fraunhofer.de (A. Willert).

https://doi.org/10.1016/j.ijhydene.2022.04.197

Accepted 20 April 2022
Available online 20 May 2022

Keywords:
Sequential deposition
Membrane
Catalyst
Ionomer
Fuel cell
Inkjet printing

membrane ionomer layer and the top catalyst layer; b) inkjet-printing of both catalyst layers onto a membrane; c) inkjet-printing of the ionomer layer as well as the catalyst layers onto the reinforcement layer of the membrane. The produced catalyst and membrane layers were characterized and proved uniform in terms of catalyst loading (0.2–0.4 and 0.08 mg_{Pt} cm^{-2} for cathode and anode, respectively), ionomer distribution and thickness homogeneity (4 μm for catalyst layers). The fully inkjet-printed CCM outperformed conventionally made assemblies in electrochemical-performance testing, even reaching 15% higher power density.

Introduction

Polymer Electrolyte Membrane Fuel Cells (PEMFC or sometimes PEFC) are on the rise to become the successor to conventional technologies for electric power generation in both stationary [1] and mobile applications [2]. As a result from constant improvement in terms of robustness and durability, PEMFC technology is expected to be extensively implemented within the next 10–15 years [3]. However, this scope can be achieved only if transition from low-volume to mass production is effectively straddled to meet the market maturity; this can be achieved by an efficient and continuous Membrane Electrode Assembly (MEA) manufacturing, with an MEA consisting of a Catalyst Coated Membrane (CCM) with a Gas Diffusion Layer (GDL) assembled on each side.

Currently, the industrial production of all the components such as catalyst and ionomer – for electrodes and membrane, respectively – is performed through independent, separate steps on decal transfer substrates, which are assembled together with the membrane only at the end of the process by tempered lamination [4,5]. Adding of GDL on both sides of the laminated CCM generates the MEA, thus ending the process [6,7]. Unfortunately, all the methods are non-continuous, which often causes non-homogeneity of the layers, local delamination, recurring defects [8] and waste of raw materials (i.e., the rather expensive catalyst and ionomer [9,10]), ultimately making production slightly less than perfect. The process of membrane manufacturing is even more cumbersome, since the presence of a permeable perforated mechanical support – expanded polytetrafluoroethylene (ePTFE) for low-temperature PEMFC and polybenzimidazole (PBI) for high-temperature PEMFC – within the membrane is required to add mechanical strength to the layer itself, otherwise consisting of the sole ionomer. The recently developed direct deposition of catalyst material onto the membrane by slot-die coating [11] partly addresses the aforementioned issues. It is carried out to form the CCM followed by adding the GDL. Although the latter also requires pressing of the GDL onto the CCM to form the MEA, cold pressing is usually sufficient [12,13] and therefore the properties of membrane and catalyst layers (e.g., porosity, tortuosity, tailored gradients) may not be altered, since exposure to high temperatures is eliminated [14].

In order to leap from a discontinuous process to continuous production, a set of innovative deposition techniques has been considered over the last decade. Notably, both coating and printing techniques have been tested for fabricating fuel cell layers in an attempt to step towards industrial roll-to-roll production: slot-die coating [11,14], knife coating [14], gravure printing [15–17], bar coating [18,19], together with screen printing [20] and inkjet printing [21,22] were employed to either manufacture a whole CCM or parts of it, mainly focusing on catalyst layers.

Compared to the aforementioned techniques, inkjet printing features a higher degree of freedom in patterning and production flexibility [23]. Accurate droplet jetting with volumes ranging from microliter down to picoliter order of magnitude can be used very precisely for dosage of functional materials deposited per unit of area onto the substrate. Typical drop volumes of drop on demand (DoD) inkjet technology lie in the range of 0.5–500 pl, corresponding to diameters of 10–100 μm [24,25], with high flexibility as a result of the firm control on droplet trajectory, which also yields to a deposition accuracy of less than 5 μm. This constitutes the remarkable advantage of inkjet over mainstream non-contact coating methods such as spray coating. Moreover, inkjet printheads do not come into contact with the substrate, yielding a better deposition in terms of shape and amount of ink released locally.

Ink formulation for each of the reviewed methods is dictated by physical principles and restrictions such as dynamic viscosity and gravimetric density that the chosen method can handle [26]. It is a prerequisite for the ink to contain targeted loading of catalyst particles and fulfill requirements in terms of catalyst/ionomer weight ratio and solid content-to-solvent ratio, with solvents being needed to stabilize the ink as a dispersion. The dispersion should also possess surface tension that is sufficiently high to prevent ink dripping from the nozzles [25]. Another main requirement is particle size in the submicrometric range be significantly smaller than 1/10 of the nozzle diameter in order to avoid nozzle clogging [27]. Notably, particle-aggregation tendency has to be suppressed to minimize clogging phenomena, thus ensuring stable jetting from the printhead nozzles during operation. This can be achieved by using appropriate additives or tailoring the ink formulation, acting on concentration of compatible solvents that feature different boiling point and volatility. Ultimately, it is a prerequisite that formulation be also chemically inert to the selected printhead and ink supply system, since swelling of plastic parts or corrosion of metal components may lead to considerable damage of the hardware and poisoning of the catalyst electrodes, hence substantially reducing the electrochemical performance [28–31].

Among the previous studies employing inkjet printing for PEMFC layer manufacturing, Taylor et al. [32] deposited aqueous catalyst inks onto GDL, realizing a loading gradient of catalyst material in the electrode. These electrodes performed comparatively better than the conventional, uniformly coated catalyst layers under the same overall platinum loading. Shukla et al. [22,33] produced thin catalyst electrodes by inkjet printing, applying low platinum loading, ranging from 0.014 to 0.113 mg Pt cm^{-2}. Scanning Electron Microscopy (SEM) [22,33,34] proved that the ink-jetted layers possess porous structure and Pt/C catalyst aggregates partially covered by the included ionomer, therefore they provide optimal three-phase interface. Different strategies to optimize the use of Pt/C catalyst through tailored gradients of catalyst content or porosity distribution were also investigated [22,35–37]. Notably, electrodes produced by inkjet printing yielded electrochemical performance comparable to those of conventionally manufactured [37]. It is reported that direct deposition of the catalyst onto the Nafion® membrane shows similar high performance, with the advantage that no post-processing, such as lamination, is necessary, thus allowing further cost reduction and production-rate increase. Recently, improvements in ink formulation also resulted in matching quantitative values of layer transport properties between inkjet-printed electrodes and those fabricated conventionally [38]. In addition to catalyst layers, inkjet printing has been used to deposit the ionomer material, especially Nafion®, as the membrane onto a catalyst layer to form the MEA in a direct deposition method. The membrane thickness governs certain transport phenomena such as back-diffusion of water and fuel crossover, therefore it impacts on fuel-cell performance to a great extent [22,39–41]. An improvement related to a different drying regime of the inkjet-printed membrane was achieved by Wang et al. [42], which resulted in more compact layers compared to those produced by spray coating.

As reported in the reviewed literature sources, separate deposition of catalyst layer and membrane layer has been investigated quite extensively at laboratory scale. As a further progress, the scope of the present work is to perform additive manufacturing of the functional layers involved by inkjet printing: both the catalyst layers (electrodes) and the ionomer layer included within the membrane were deposited through industrial fabrication strategies, then compared to lab-scale experiments [43]. An experimental approach was developed and realized for multilayer inkjet printing, as inspired by recent contributions [44,45]. The whole effort can pave the path to future implementation of the proposed methodology by MEA manufacturers in the context of scaling up volumes together with increasing layer quality. Ultimately, the outcomes from this research may serve as a foundation towards a more cost-effective and roll-to-roll CCM production.

Experimental setup and methodology

Experimental set-up and general conditions of the experiments

Inkjet-printing experiments were conducted at lab scale, employing a commercial printing equipment, the *Digital Materials Printer DMP-2831* by *Fujifilm Dimatix*. It is a stand-alone inkjet-printing system designed for proof of concept and rapid prototyping in laboratory-benchtop mode. This inkjet printer features high versatility, as it is capable of jetting a variety of inks (i.e., aqueous, alcohol based, UV-curable, solutions and dispersions). High chemical compatibility is associated with the employed silicon nozzles (nozzle diameter of 21.5 μm). For instance, it is widely used for scientific and technical research in printing electronics, e.g. for certain conductive inks [46,47]. It is worth noting that the selected printer is capable of producing samples at relatively low speed, due to the limited number of nozzles and the small droplet volume: 16 nozzles compared to typical pilot and industrial printheads endowed with 256–2048 nozzles and droplet volume of 10 pl maximum compared to 50–80 pl for industrial printheads. As a reference, printing a single sample of 50 mm × 50 mm may require up to 6 h, depending on the number of operated nozzles and the number of deposited layers.

As previously shown for electronics applications [46,47], a variety of inks loaded with solid nanoparticles are currently processed by similar printing machines. Therefore, the deposition of catalyst layers is also feasible, since Pt/C particles are usually of size between 100 nm and 1 μm [48]. Ink printability is determined by fluid properties: viscosity, particle loading and particle-size range are dictated by nozzle diameter and chemical compatibility. So, limitations of the selected printing machine, such as small nozzle diameter or relatively low deposition rate, should not be mistaken for general disadvantages of the inkjet-printing method. The employed printhead is able to process solid particles of about 1 μm maximum size; however, it is recommended that particle size be in the order of $1/100^{th}$ of the orifice diameter (about 200 nm as the optimal value) [27,49]. Moreover, as mentioned in the previous section, ink viscosity is limited by the inherent constraints of the implemented technique and shall be ideally near to 10 mPa s (12 mPa s maximum) at 60 °C, which is the maximal operating temperature of the printhead. As additional requirements, pH in the range 4–9 and a surface tension between 28 and 33 dyn cm^{-1} is preferable.

Droplet spacing – a key parameter in inkjet printing – is the distance between a generic droplet and the next one along a generic coordinate and is used to determine the number of droplets per unit area, thereby defining the catalyst loading of the sample as the result of deposited ink volume per unit area. Typically, a Cartesian coordinate system is projected onto the substrate, with *x* axis corresponding to the carriage direction (i.e., the direction along which the printhead moves) and *y* axis being perpendicular to the former. In piezo-driven DoD inkjet printing, a waveform editor allows tuning the electronic pulses to govern the piezo actuator inside the printhead and ultimately govern the jetting of ink droplets. So, the timing between moving speed of the printhead and two consecutive pulses is the parameter governing droplet spacing over the target substrate along the *x* axis, together with indirectly imposing type and frequency of nozzle-cleaning cycles. Therefore, timing and voltage of the waveform and other cartridge settings can be actively adjusted while monitoring droplet formation to attain the desired spacing. The angle of inclination of the printhead with respect to the carriage

direction, the Sabre angle α_s, needs to be adjusted manually to impose the desired droplet spacing along y axis. In summary, pulse frequency, moving speed of the printhead and Sabre angle are the three parameters that determine print resolution, since nozzle spatial distribution within the printhead is fixed. Table 1 reports resolution and droplet spacing as a function of Sabre angle for the selected inkjet printer. In the selected printing machine, drop spacing is adjustable between 5 μm and 254 μm. The procedure of drop spacing optimization by adjusting pulse frequency and inclination angle is carried out for each deposited ink separately, depending on the different ink properties and the layer characteristics to be attained.

The employed printing system can print patterns up to 200 mm × 300 mm on its tempered vacuum platen. Hardware and software were not customized for the experiments involved in the present research. It is worth remarking that scaling up to mass production may imply redesigning and modifications of some technical aspects; however, the developed approach to inkjet-printing of fuel cell layers may be employed as is in assembly lines featuring industrial printers, since similar designs and concepts are involved.

Experimental procedure for layer deposition

In the conducted experiments, dispersions containing Pt/C catalyst and ionomer, as well as inks containing only ionomer were employed; they were nearly identical to those typically used for deposition of electrode active layers and membrane layers. The detailed formulation of catalyst inks and the procedure to prepare them is proprietary of *Johnson Matthey Fuel Cells*. In general, the core of catalyst inks is an elaborate formulation of Pt/C agglomerates, ionomer, distilled and deionized water, and/or alcohols. The inks may also contain negligible amounts of surfactants, chelating agents and binders to tune viscosity and colloidal stability. Cathode inks with a solid content in the 10–20 wt% range, anode inks with a solid content in the 5–15 wt% range and an ionomer dispersion with a solid content in the 15–25 wt% range were used in the conducted experiments. As for viscosity, all the employed inks exhibit values around 20 mPa s: as measured by Santangelo et al. [50] over the 1000–15,000 s^{-1} range of imposed shear rate for three representative inks, viscosity of the ionomer solution is between 20 and 25 mPa s, while ranging from 10 to 20 mPa s for catalyst inks. It is also worth remarking that those inks generally exhibit Newtonian behavior.

Table 1 – Resolution characteristics of the *DMP-2800 Series* inkjet-printing machines by *Fujifilm Dimatix*.

Resolution [dpi]	Sabre angle α_S [°]	Droplet spacing [μm]
5080.00	1.1	5
2540.00	2.3	10
1693.33	3.4	15
1270.00	4.5	20
1016.00	5.6	25
846.67	6.8	30
317.50	18.4	80
203.20	29.5	125
100.00	90.0	254

In order to provide proper functionality of catalytic layers, certain microstructural characteristics, such as porosity, are to be properly set. Particle size, distribution network of the ionomer and drying procedure are the main factors determining porosity. As mentioned in Subsection 2.1, a prerequisite for inkjet printing is making ink viscosity and solid-particle size fall within ranges suitable for the printhead. For the ionomer ink, these requirements are generally met, but the catalyst inks may feature relatively higher viscosity and larger particle size than the recommended values. As for viscosity, all the employed inks exhibit values around 20 mPa s. With regard to the solid content, the characteristic D_{90} of Pt/C agglomerates (i.e., representative particle size larger than 90% of the particles in the ink) was in the order of 1 μm. So, ink viscosity and particle size are at the limits of the operative ranges suggested for this type of printing machine. In general, a solid content with higher D_{90} could be more beneficial, but for the sake of printability inks with lower D_{90} were used. Smaller Pt/C ratio may generate a denser layer instead, also reducing its porosity and therefore performing poorly from an electrochemical standpoint.

At the beginning, the substrates for catalyst ink deposition were PTFE sheets and subsequently ionomer membranes. Finally, additively-manufactured intermediate production layers were used. They were either held by the vacuum platen or constrained within a customized rigid frame. The active surface of the electrode layers was 52 mm × 52 mm for the anode and 50 mm × 50 mm for the cathode. Overall, the experiments were conducted at room temperature; both the printhead and the substrate were kept at 28 °C, with drop spacing set between 5 μm and 15 μm. As described in Subsection 2.1, waveform and Sabre angle (Table 1) were modified for each tested deposition to achieve the following nominal targets in terms of layer characteristics: average catalyst content over the entire active surface of 0.3 mg Pt cm^{-2} and 0.1 mg Pt cm^{-2} for cathode and anode, respectively; 8 μm–14 μm thickness for catalyst layers after drying. In the light of these target values, the desired drop spacing in depositing the anode layer was evaluated as 12 μm–15 μm and as 5 μm in cathode-layer deposition, with single-pass printing for each of the electrodes. For the ionomer deposition, a 2-pass printing was performed instead.

Nozzle clogging was observed during printing experiments when catalyst ink was involved, even though the solid content of the employed inks was lower than the suggested value of 25 wt% [49,51]. This phenomenon is rather common in inkjet-printing of functional materials, since the liquid phase partly evaporates prior to droplet release. If the solvent is very volatile, this results in solid particles remaining attached to the nozzle and nozzle-plate walls, thus obstructing ink flow. The unwelcome effect caused poor quality of the printed layers with missing lines and missing spots; the extent of that tends to deteriorate throughout the experiment, since more nozzles are affected. Therefore, the longer the printing time, the more artefacts may occur on deposited layers. This issue was addressed by making relative humidity increase at the nozzle outlet: to this end, a water/alcohol-soaked tissue was added, an approach known as "vapor trap". This approach turned out as effective and was applied in the whole experimental campaign. From a chemical standpoint, other strategies to limit clogging

have been suggested and developed [52,53], which mainly consist of including additives that exhibit very low tendency to evaporate (e.g., glycol-based compounds). However, this approach was not adopted in the present work, as the included chemicals remain in the catalyst layer even after the final drying and have a detrimental effect on the performance. Lengthy non-operating periods of either individual nozzles or the entire printhead may also cause clogging.

Approach to multilayer printing

Multilayer and sequential deposition, the ultimate goal of this work, was performed by implementing three different approaches that were developed as based on the experience and the results obtained while depositing single layers. Fig. 1 shows a sketch presenting the workflow of the first strategy, called "CCM on carrier".

In this bottom-to-top printing approach, the first catalyst layer – either the anode or the cathode, since the deposition order was determined as irrelevant through this methodology – was coated onto a PTFE carrier substrate (Fig. 1A) by slot-die coating. On top of this dried layer, the ionomer was deposited by inkjet printing to generate the membrane (Fig. 1B) and then let dry. As a mere drawback of handling the involved layers manually, it was not possible to include the ePTFE reinforcement layer (Section Introduction) into the wet ionomer layer, but the inclusion would be feasible if the process were automatized. As the last step, the second catalyst layer (Fig. 1C) was also deposited by inkjet printing and let dry. The result was a full CCM on top of a PTFE carrier substrate, available for further processing.

The second approach, called "floating CCM", was devised to generate a CCM starting with a commercial Nafion® 115 membrane (125 μm thickness) without employing any carrier substrate (Fig. 2), thus being mechanically more complex.

In a pre-processing step, the seal frame was applied to the membrane after the membrane had been fixed inside a rigid frame. It is worth clarifying that the seal is not a functional layer for the chemical reaction involved [43] and its manufacturing exceeds the scope of the present work. The seal-membrane assembly remained firmly stabilized in the used frame (Fig. 2A). Subsequently, the first catalyst layer was deposited by inkjet printing within the existing seal frame (Fig. 2B) and let dry. After drying was completed, the whole sample was turned over and the second catalyst layer was printed onto the uncoated side of the membrane to form the counter electrode (Fig. 2C). After the final drying process, the resulting CCM could be removed from the mounting frame and further processed (Fig. 2D).

The third approach, called "ePTFE CCM", is presented in Fig. 3, arguably the most complex at lab scale, but very promising for industrial production.

It is also the most comprehensive one, since it includes full forming of the membrane. It starts one step earlier than "floating CCM" (Fig. 2): instead of starting from a complete membrane, the ePTFE reinforcement layer (2 μm–5 μm thickness) was fixed inside a rigid frame and was employed as the seed layer. Moreover, in this method the seal frame was manufactured as a preliminary step in the workflow to add mechanical stability. The whole seal-reinforcement carrier remained inside the frame (Fig. 3A). In the first printing cycle, the ePTFE layer was impregnated with the ionomer ink by inkjet printing on both sides to generate the membrane (Fig. 3B) and let dry. On both sides of the printed membrane, the catalyst layers were deposited by inkjet printing one after another (Fig. 3C) and let dry. Finally, the fully inkjet-printed CCM could be removed from its frame and further processed (Fig. 3D).

The overall approach proposed here falls within the realm of additive manufacturing as defined by a recognized standard, since materials are added together *"layer upon layer"* to form a monolithic functional device [54]. Notably, the three

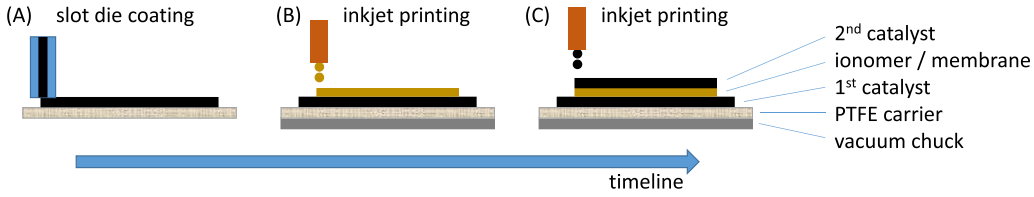

Fig. 1 – CCM on carrier: additive manufacturing onto PTFE carrier; (A) slot-die coating of the first catalyst layer; (B) inkjet printing of the ionomer to generate the membrane; (C) inkjet printing of the second catalyst layer.

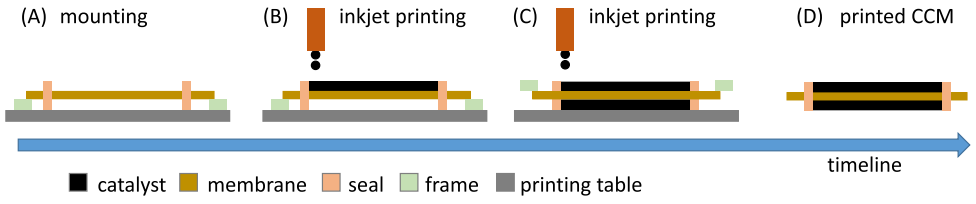

Fig. 2 – Floating CCM: additive manufacturing onto membrane; (A) mounting of the membrane for inkjet printing; (B) inkjet printing of the first catalyst layer; (C) inkjet printing of the second catalyst layer; (D) CCM finished and detached.

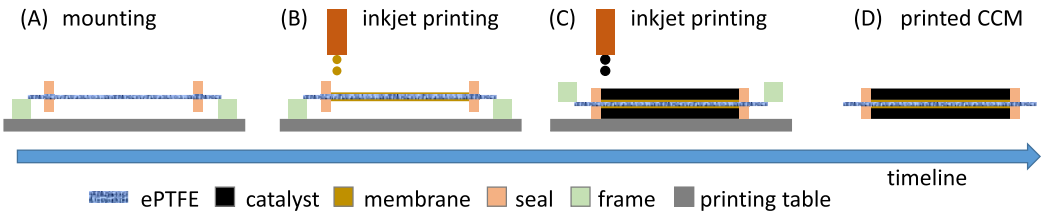

Fig. 3 – ePTFE CCM: additive manufacturing onto ePTFE; (A) mounting of ePTFE for inkjet printing; (B) inkjet printing of the ionomer to form the membrane; (C) inkjet printing of the catalyst layer; (D) CCM finished and detached; steps (B) and (C) are performed on both sides of the reinforcement layer.

developed methods exploit additive manufacturing to an extent that varies from depositing the sole catalyst layers to depositing all the layers included in a CCM.

Evaluation of layer characteristics and performance

A set of X-ray fluorescence spectroscopy (XRF) measurements was conducted on the single layers, mainly to assess how the target amount of catalyst and the target thickness were met by the inkjet-deposited layers; the employed device is an *X-MET8000* analyzer by *Hitachi High-Tech*. Moreover, optical microscopy analysis of both, single layers and multilayer assemblies, was carried out employing a *KH-8700* 3-dimensional digital microscope by *Hirox* to detect defects that may arise as final drying is completed. Electrochemical performance analysis was also conducted to ultimately compare the CCM manufactured by the approaches described in Subsection 2.3 with those conventionally made.

Thickness measurements were performed employing a *Dektak 150* stylus surface profilometer by *Veeco* to evaluate dry-layer thickness. For the characterization over the whole surface, three measurements were made in different regions of the printed catalytic layers with a ±0.4 μm resolution and a measurement range of 65.5 μm on a scan length of 4.5 mm. Acquisition of data points started on the uncoated PTFE substrate to investigate the transition from substrate to printed catalyst layer, thus even assessing the quality of the printed edges of the layer.

Tests for electrochemical performance of the fuel cell were conducted using FuelCon test bench with test cell fixture quickCONNECT qCf FC25 by BalticFuelCells GmbH and Solartron Modulab potentiostat booster 12 V/20 A by AMETEK, Inc. For the electrochemical measurements, activation and break-in of all the cells were performed with a standardized protocol implementing the recommendation of the Fuel Cell and Hydrogen Joint Undertaking (FCH JU) EU harmonized test procedure. Few modifications based on the goals and requirements of the project were applied. The polarization curves were measured under the conditions that are near to realistic operation requirements of such in mobility application.

Results and discussion

Single layers

A preliminary analysis on the inkjet-printed single layers was carried out to better assess and optimize the setup of the printing experiment (Subsection 2.1). Some tests were both quantitative and qualitative, whereas others were aimed at

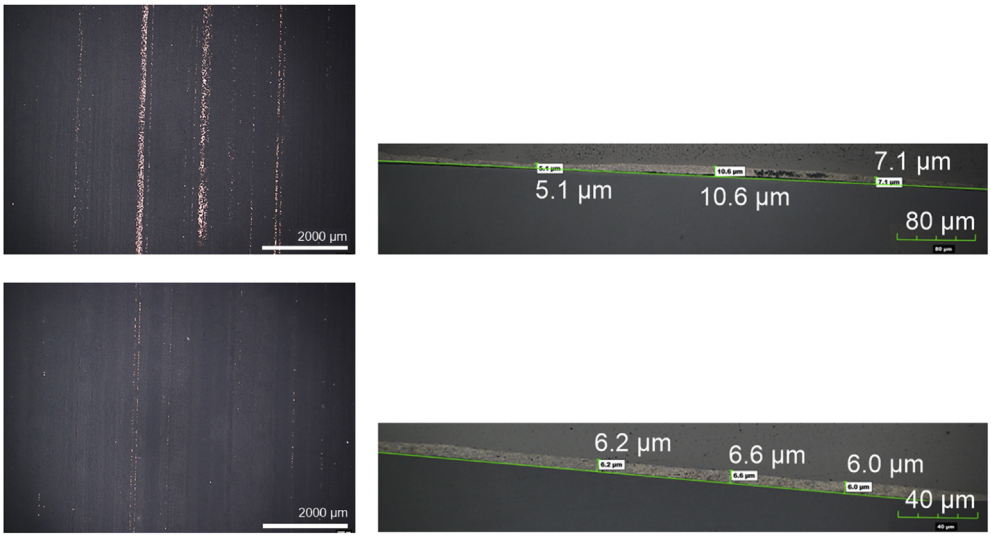

Fig. 4 – Catalyst layer (anode) under optical microscopy with backlight illumination (left) and scanning electron microscopy (SEM) (right); top: sample with many defects originated by nozzle clogging; bottom: sample of better quality.

evaluating how the layers met specific target values reported in Subsection 2.2 with regard to chosen parameters.

Firstly, a simple assessment of the catalyst layer quality was made by back-illuminating a single printed layer. This very practical approach allowed emphasizing the negative effects of nozzle clogging on the quality of dried printed layers (Subsection 2.2): Fig. 4 shows a typical result, mainly highlighting the comparison between a less-than-perfect layer (Fig. 4, top) and an improved one (Fig. 4, bottom).

Several defects are known to occur and limit the performance of a functional layer, typically pinholes, cracks and delamination [8]. Nozzle clogging throughout printing made missing material clearly visible by back illumination in Fig. 4 (top left), where a continuous series of pinholes along vertical lines (characteristic size of up to 10 μm per each hole, about 10 lines over the whole printed area) yielded the undesired "starry night"-like defect, also typical of stress-induced flaws in polymer films [55]. That prompted the implementation of anti-clogging strategies, as the vapor trap described in Subsection 2.2, which resulted in remarkably improved layer quality (Fig. 4, bottom left). As shown, some pinholes along a few lines still occurred though, which might be inherent and arguably more related to drying stresses or missing individual droplets; however, the presence of pinholes along vertical lines suggests that clogging mildly affected deposition, thus requiring further effort. A SEM analysis of the two previously tested layers was also conducted, focusing on their cross section. As shown in Fig. 4 (top right), thickness inhomogeneity [8] occurred in the poorly deposited layer, ranging between a maximum of 10.5 μm and a minimum of 6 μm. Conversely, the bottom right image of Fig. 4 exhibits a practically constant thickness of anode sample, nominally equal to 6 μm.

Subsequently, the Pt-loading was investigated by XRF analysis on the catalyst layers, printed with anti-clogging measures. Fig. 5 shows the results from that test for a set of samples of both electrodes (above/below picture with nominal loading of 0.1 mg_{Pt} cm^{-2}/0.3 mg_{Pt} cm^{-2}).

The results highlight an overall effective ability of the printing technique and devised approach to achieve target values (Subsection 2.2) as an average over the active surface. In addition, local deviations from target values and general inhomogeneity of the printed layers in terms of catalyst loading can be identified. It is worth noting that homogeneity along the printing direction (carriage direction, x axis in Fig. 5) is rather high, with a maximum deviation from the average of ±0.005 mg_{Pt} cm^{-2}. However, larger fluctuations are apparent along the coordinate perpendicular to the printing direction (y axis in Fig. 5), with a maximum deviation of ±0.05 mg_{Pt} cm^{-2}. The ultimate reason for this discrepancy lies in the inhomogeneous layer thickness, mainly resulting from non-constant amount of deposited material due to partial nozzle clogging. Therefore, a combined approach to correlate Pt-loading with deposition parameters was implemented, which consisted of evaluating layer thickness by SEM analysis of the cross-section, since catalyst loading is proportional to the thickness of the dry layer [56]. Notably, Fig. 6 shows the results from SEM analysis of both the anode and the cathode: in both samples a clear variation of the layer thickness can be identified, ranging between 7 μm and 8 μm for the former and between 9 μm and 10 μm for the latter.

As previously observed about Pt-loading, this inhomogeneity is arguably due to spatially variable deposition, even though drying conditions may also have an impact on that. Overall, the correlation between layer thickness and Pt-loading of the samples seems relatively evident: in the

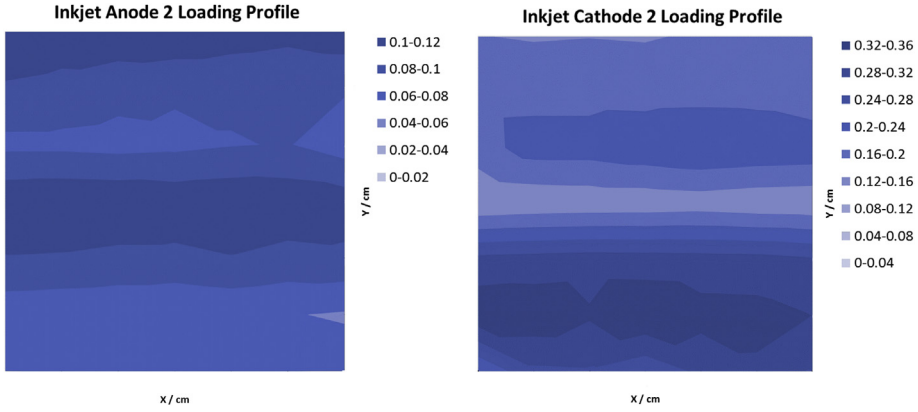

Fig. 5 – Pt loading profile of inkjet-printed single catalyst layers. Left: anode layer (target: 0.08 mg_{Pt} cm^{-2}, average: 0.089 mg_{Pt} cm^{-2}, minimum: 0.058 mg_{Pt} cm^{-2}, maximum: 0.120 mg_{Pt} cm^{-2}); right: cathode (target: 0.2–0.4 mg_{Pt} cm^{-2}, average: 0.230 mg_{Pt} cm^{-2}, minimum: 0.123 mg_{Pt} cm^{-2}, maximum: 0.356 mg_{Pt} cm^{-2}).

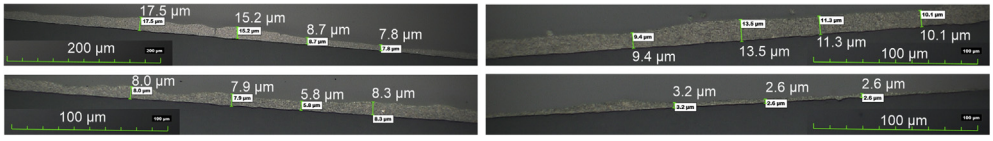

Fig. 6 – SEM analysis of the inkjet-printed catalytic layers: cross-section of anode (left) and cathode (right).

regions where layer thickness was lower than the target value, so was the catalyst loading.

The reported analysis prompted a further optimization of printing parameters to obtain more homogeneous layers without compromising the average Pt-loading, which proved consistent with the target values for both electrodes. To this end, action on drop spacing was taken, since the volume of material deposited onto the substrate to generate the layer is related to the inverse drop spacing to the power of two [57]. This relationship provided a guidance to obtain an optimized drop spacing for achieving a more uniform Pt-loading. From a practical standpoint, that implied a combined action on both Sabre angle and frequency of the firing signal (pulse frequency in Subsection 2.1). Moreover, duration and type of cleaning cycles were also adjusted, since they are mostly run through sub-firing signals that occur between two consecutive droplet releases. As mentioned in Subsection 2.2, it was observed that deposition at room temperature is also effective for the catalyst inks and yielded optimal printing results. After implementing the abovementioned adjustments to drop spacing, further analysis of the printed samples was conducted by XRF for specific element mapping: a more homogenous and consistent catalyst distribution over the active surface of both anode and cathode layers was proved in comparison with the previous set of samples. Finally, Pt-loading consistency with target values appears overall achievable by inkjet printing, with small fluctuations along the printing direction and along the direction perpendicular to that.

A less demanding layer in terms of performance requirements, the ionomer layer was mainly analyzed by profilometry. Notably, three samples were tested to evaluate layer thickness of the ionomer solution described in Subsection 2.2 and deposited onto a PTFE substrate in multipass (i.e., 2-pass) printing mode. An average thickness was detected as about 4 μm, with variation over the whole surface yielding roughness that could be even visually identified. In spite of maximum spatial deviation of 1 μm over each individual sample and 0.5 μm between samples over all the measurement points, it appears that inkjet printing under the selected printing approach was generally capable of meeting the target thickness. It is worth remarking that the produced samples are mostly a proof of concept, since the typical thickness of PEMFC membranes lies between 10 μm and 50 μm [58–60].

Multilayer structures

The analysis of multilayer assemblies produced by the inkjet-printing approach described in Subsection 2.3 was performed mostly by optical microscopy and SEM evaluation against the produced samples. The first multilayer manufacturing method (the "CCM on carrier", Fig. 1) consisted of inkjet-printing the ionomer and a catalyst layer onto a pre-manufactured, slot-die coated catalyst layer. These samples have not been ultimately tested in terms of electrochemical performance, since the "CCM on carrier" approach is mostly focused on optimizing deposition. Some optical-microscopy images of the sample surface are shown in Fig. 7, with printing direction being from left to right: as the main drawback of this method, the analysis revealed missing lines (i.e., series of pinholes along a line) and cracks occurring over the top, inkjet-printed catalyst layer. Notably, Fig. 7a and c presents only the catalyst layer inkjet-printed on top of the ionomer. As already remarked in Subsection 3.1, the use of backlight generally makes defects and particularly missing material become more easily detectable. The defects shown in the images were most likely caused by high tensile stress within the multilayer assembly during the drying process. Since

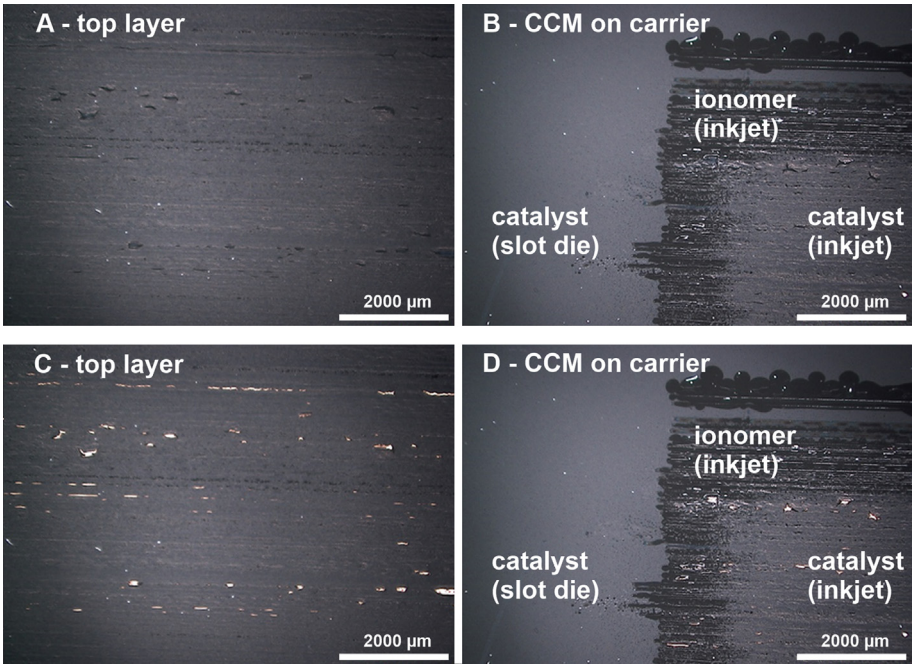

Fig. 7 – Microscopy images of a multilayer structure generated by the "CCM on carrier" approach, without (A, B) and with (C, D) back light: A, C) top inkjet-printed catalyst layer; B, D) all sequentially printed layers.

during drying of the ionomer ink on the previous catalyst layer drop pinning exerts negative hydrodynamic pressure on the substrate causing partial delamination and formation of pinholes and since nozzle clogging had been almost fully addressed by dedicated strategies, the visualized defects are believed to be mainly due to drying dynamics (Subsection 3.1).

In Fig. 7 surface roughness can be seen. However, attaching of a GDL layer in actual operating conditions would imply exerting pressure on top of those rough surfaces, which would result in properties not being significantly changed, since applying pressure is well-known as a mechanical strategy to reduce undesired additional resistance – both thermal and electrical – induced by irregularities.

Fig. 7b and d presents the full assembly. The alignment of the various layers was shifted as they were sequentially deposited (i.e., ionomer, followed by the second catalyst layer) to clearly distinguish the respective edges, thus allowing a visual assessment of the edge quality of the inkjet-printed layers. Therefore, there is no straight border of the ionomer layer, due to slight misalignment of the printhead once a new line starts. A separate stripe of material was printed on top of the ionomer layer as a reference printing test, without being aimed at serving for evaluation purposes. Stripes within the ionomer layer are clearly visible in both Fig. 7b and d, which hint at additional stress-related defects. Another effect clearly visible in Fig. 7c and d is that the inkjet-printed ionomer layer tends to cause some shift of the materials constituting the slot-die coated catalyst layer placed underneath (i.e., delamination). Although there were no initial defects in the slot-die coated layer itself, Fig. 7d highlights defects in the region where the ionomer overlaps it by the incoming light through the layer. This might be due to the inherent porosity of the catalyst layer, necessary to perform gas diffusion: the inkjet-printed, wet ionomer ink may penetrate the pores of the already dry catalyst layer (i.e., the slot-die coated one) and partially dissolve into it.

Further investigation of the multilayer cross section by SEM revealed regions where remarkable variation of the ionomer thickness occurred, spanning from about 8 μm to 20 μm (Fig. 8).

On the other side, the inkjet-printed catalyst layer featured a rather constant thickness, which hints at successful deposition. As an additional consequence of the inhomogeneous thickness of the ionomer layer, undesired direct contact between the first (i.e., the base) and the second (i.e., the inkjet-printed) catalyst layer was locally detected in cross-sectional images (Fig. 8), as well as in those taken from the surface (Fig. 7b and d). This effect will cause the CCM to have electrical shorts and make performance decay almost immediately. It is worth stressing that adhesion of the catalyst layer on PTFE is weak and therefore PTFE is used as decal substrate. Once ionomer is deposited to form the membrane and during the drying process, drop pinning and drying dynamics make the ionomer layer exert enough force on the catalyst layer to detach and delaminate it from the layer lying underneath. Although there were some strategies employed to hamper this effect during ionomer printing, the effect could not be fully obviated once the final layer of counter electrode was deposited. So, it can be observed that this effect cannot be completely avoided if decal transfer substrates with low adhesion are used for deposition.

The proposed approach is overall feasible and yielded to full CCM assemblies, yet the quantitatively significant variability of ionomer thickness, the defects occurred in both the inkjet-printed layers – generally identified as delamination – and the local penetration of ionomer into the dry catalyst layer prompted to devise some improvements. Mechanical strength of the ionomer layer could be increased by applying a reinforcement film on top of the inkjet-printed ionomer layer, thus also limiting penetration into the dry layer and avoiding direct contact between the two catalyst layers. An additional strategy to improve the homogeneity of the ionomer layer consists of reducing the concentration of the ionomer powder within the ink (i.e., a solution) to increase its handling properties. As an example of its implementation, Fig. 9 shows a series of ionomer inks with varying solid content (2.5–20 wt%) deposited onto a slot-die coated catalytic layer. This approach to generate the membrane has been also been described by Breitwieser et al. [40]. In his investigations this inkjet printed membrane was in a fuel cell more powerful than a reference membrane.

Improvement in layer homogeneity was detected by reducing the solid content down even to 10 wt%. As an obvious consequence, reduction of the solid content implies an increase in the number of printing cycles (i.e., multi-pass operation) to deposit the same amount of ionomer. Along this line, an even further reduction of the solid content to 2.5–5 wt% led to fully eliminate nozzle clogging and therefore to reduce the required cleaning cycles. However, the number of printing times had to be increased proportionally to the decrease of the solid content, which made select the 15–25 wt% range (Subsection 2.2) as the optimized condition combining layer quality and production time.

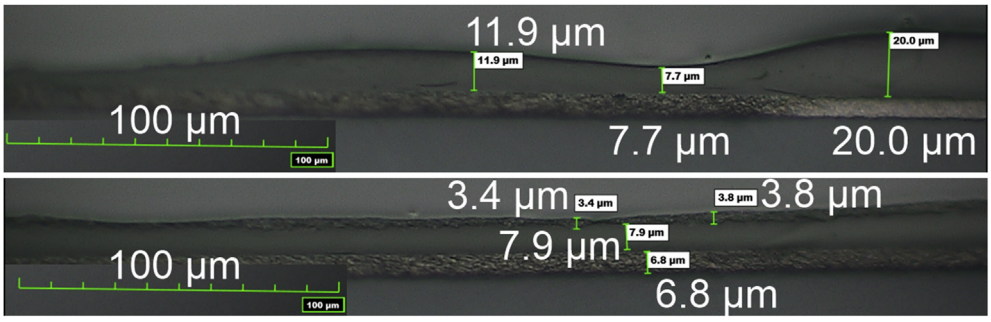

Fig. 8 – SEM images of the cross section of a multilayer structure generated by the "CCM on carrier" approach.

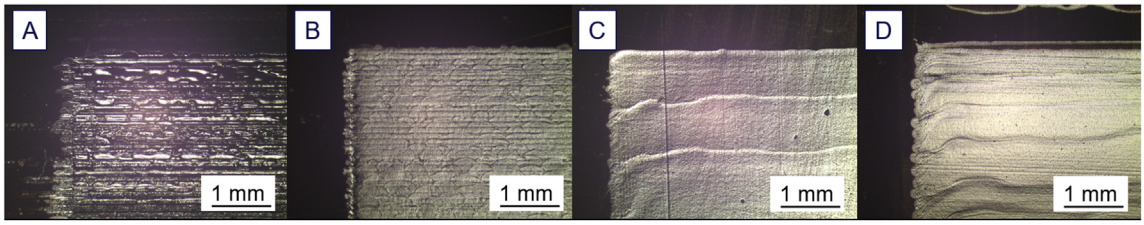

Fig. 9 – Ionomer layer under different ionomer concentrations within the deposited ink: a) 20 wt%; b) 10 wt%; c) 7.5 wt%; d) 2.5 wt%.

In the approach "floating CCM", inkjet-printing of the catalytic layers was performed directly onto the reinforced membrane (Subsection 2.3), with the seal layer being deposited onto both sides of the membrane in a preliminary step, which served as a reinforcement for the subsequent filling with catalyst inks. The printed samples are shown in Fig. 10, which includes both the individual catalytic layers and the full CCM assembly.

As expected in an inkjet-printing procedure that only involves the catalytic layers, the issues previously reported about the "CCM on carrier" approach were barely apparent through the present one, thus obtaining layers with rather homogeneous thickness and almost flawless in terms of defects. However, the drying process – occurred at ambient temperature – of these layers caused some tension within the membrane, resulting in generic waviness of the full assemblies. So, the membrane was fixed into a frame as an additional step of the whole approach (Fig. 2) to balance that tensile stress.

The "ePTFE CCM" approach was finally pursued as an almost full additive manufacturing of the CCM, since it started from an ePTFE support – the thin polymeric ePTFE film – fixed to a carrier frame, onto which inkjet-printing of ionomer and catalytic layers was carried out (Subsection 2.3). The results from the first step (i.e., inkjet-printing of the ionomer to generate the membrane) is shown in Fig. 11.

Ionomer deposition was performed onto both sides of the ePTFE substrate, implementing the strategies previously suggested to avoid inhomogeneous thickness and undesired stress-related delamination through drying: an optimized ionomer concentration was set in the deposited ink and a frame was applied as a constraint. Moreover, letting the membrane dry prior to catalyst-ink printing allowed addressing ionomer penetration within the catalytic layers. Therefore, the produced membrane was structurally comparable to the commercial one used for the "floating CCM" approach in terms of homogeneity and defects; ultimately, the resulting assembly proved to be homogeneous in terms of thickness and material distribution on the active surface. Therefore, this effort showed additive manufacturing of a whole CCM by inkjet printing is feasible

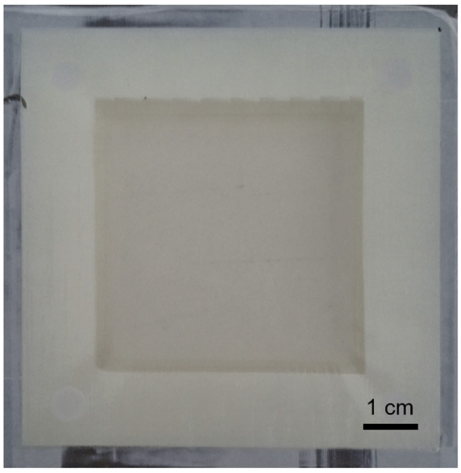

Fig. 11 – ePTFE support with seal and inkjet-printed ionomer.

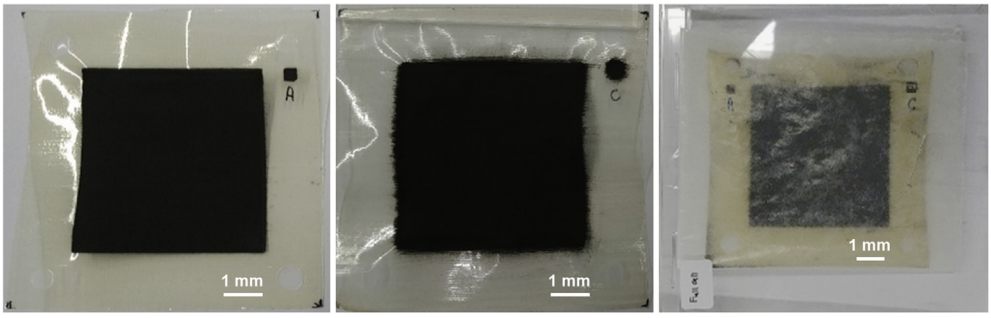

Fig. 10 – Inkjet-printed catalyst layers onto the membrane by the "floating CCM" approach; left: seal frame and printed anode layer; center: seal frame and printed cathode layer; right: CCM with printed anode and cathode catalyst layer (covered in storage container).

and effective, provided that carrier frames be employed to balance tensile stress within the ionomer layer and drying of the membrane be allowed prior to catalytic-ink deposition.

Evaluation of the electrochemical performance

As reported in Subsection 2.4, the electrochemical performance achieved by a CCM manufactured by inkjet printing through the "ePTFE CCM" approach is presented in Fig. 12, which shows polarization curve and power density of a PEMFC with that in its core as functions of current density. As the most innovative one, we deemed its resulting samples were to be challenged against conventionally made ones in terms of electrochemical performance. Full additive manufacturing of the assembly embodies the actual novelty. A comparison is also displayed against a PEMFC including a conventionally-made CCM (provided by *balticFuelCells* [61,62]), which serves as a reference to assess how inkjet printing is capable of meeting PEMFC standard output. Both MEAs consist of 0.4 mg_{Pt} cm^{-2} for anode. The reference has 0.2 mg_{Pt} cm^{-2} for cathode while the printed one has 0.1 mg_{Pt} cm^{-2}. The reference uses a Nafion 212 membrane. The printed MEA has about 50 μm membrane built from Nafion D521. The measurement conditions are 60 °C and 80%$_{RH}$ for both investigations. There is only a deviation for the cathode testing conditions in the reference cell which used 100%$_{RH}$.

The performance of the fully inkjet-printed CCM compared to the reference is very similar in power density for current densities lower than 800 mA cm^{-2} (a region of the polarization curve where Ohmic losses are predominant [43]). Some slight difference in terms of losses occurred as current density increased beyond 800 mA cm^{-2} towards the very end of the curve (the region of the polarization curve where mass-transport losses are predominant [43]). Consequently, the comparison between power-density trends appears to favor the inkjet-printed CCM over the conventionally made one, even though the two curves almost collapse onto each other

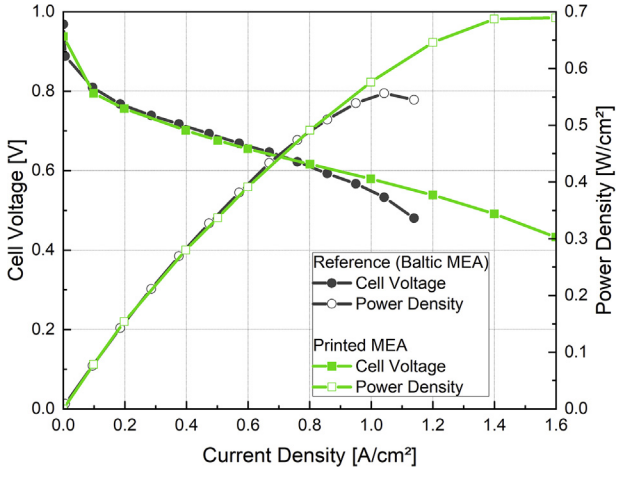

Fig. 12 – Electrochemical performance (polarization curve and power density) of a CCM inkjet-printed by the "ePTFE CCM" approach compared to a standard reference MEA by *balticFuelCells* at the same operating conditions [61,62].

over a large range of current density. As shown in Fig. 12, the peak of power density exhibited by the inkjet-printed CCM is about 15% higher than that featured by the one used as a term of comparison. This observation should be put into the context of preferably avoiding fuel-cell operation in the region where mass-transport losses are predominant (i.e., at the higher current density). However, if the same operating conditions apply, as in the case of the proposed comparison, diffusion through the involved layers ultimately governs mass-transport losses. As investigated by Larbi et al. [63], porosity has a main impact on diffusion: the two tested cells may have different average porosity, also exhibiting different degree and density of defects, which also affects mass transport.

Overall, it appears that instances of increased resistance and mass-transport losses due to local defects (e.g., pinholes [64]) do not imply the inkjet-printed CCM underperforms with respect to conventional assemblies. This result supports the feasibility of employing inkjet-printing for the manufacturing of CCMs.

Conclusions

In the present research, an approach to additive manufacturing of PEMFC layers by inkjet printing was devised and developed. The focus was set on the functional layers (i.e., catalytic layers and membrane layer) that constitute a CCM.

As an arguably unprecedented contribution, three approaches were developed and implemented for multilayer manufacturing, with variable degree of involvement of inkjet printing: a slot-die coated catalytic layer served as the foundation layer for the first strategy, with ionomer layer and second catalyst layer being sequentially deposited by inkjet printing on top of the slot-die made surface; another approach that started from a commercial membrane as the substrate for catalyst layer deposition was then devised and realized; finally, inkjet printing of all the three involved layers was performed in the third methodology, with the membrane reinforcement layer (i.e. an ePTFE film) serving as the initial substrate.

Thickness homogeneity and presence of defects were considered to quantitatively assess how successful multilayer deposition was through each tested approach. The inkjet-printed membrane layer proved the most challenging: its thickness was nominally of 8 μm, yet a variability in the order of 1 μm tended to occur. Inserting the reinforcement layer in the membrane appears instrumental in achieving a configuration where no direct contact between catalytic layers occurs; an optimized concentration of the ionomer in the ink to be deposited is also recommended to both control the related dry-layer thickness and avoid an excessive use of multi-pass mode. Even more importantly, the drying process of the ionomer layer should be carried out prior to catalyst-ink deposition to prevent the former from partially dissolving into the catalytic layer. If not carried out properly, either part of the catalyst layer would sink in the membrane or the counter electrodes would come into contact with each other and make electric shorts arise. A carrier frame constraining the membrane may also be employed during the printing process to

avoid waviness and to add mechanical stability of the membrane during deposition. On the other hand, a uniform catalyst-layer thickness was achieved more easily, being nominally equal to 4 μm, with variations in the order of 0.1 μm. However, a combined action on pulse frequency and Sabre angle had to be implemented on the printing procedure to achieve variability lower than 0.01 mg_{Pt} cm^{-2} with respect to the nominal target values of Pt-loading (0.08 and 0.2–0.4 mg_{Pt} cm^{-2} for anode and cathode layer, respectively) over the whole active surface.

Overall, all the three manufacturing routes proved rather effective. Selecting for testing in fuel cell the last – and most inkjet-printing intensive and therefore most innovative one – one ultimately competing closely and slightly outperforming against the conventionally manufactured CCM in terms of voltage losses and power density for current densities higher than 800 mA cm^{-2}: peak power density was about 15% higher which might be accounted to a different average porosity. It is worth remarking that at current density lower than 800 mA cm^{-2} both CCMs exhibit nearly the same performance, with negligible difference in the polarization curve. The comparison highlighted consistency between the two assemblies, with the performance of the inkjet-printed CCM not being penalized by higher resistance or higher mass-transport losses locally occurring as a result of defects. A deeper understanding of electrochemical performance and durability performances has to be covered as subject of further studies.

This work shows that CCM additive manufacturing by inkjet printing can be at the forefront in the transition of fuel-cell industry from small-volume to mass production, even considering the consistent quality that the tested printing technique can provide at large scale.

Declaration of competing interest

The authors declare that they have no known competing financial interests or personal relationships that could have appeared to influence the work reported in this paper.

Acknowledgments

The authors wish to acknowledge the financial support by FCH JU (Fuel Cells and Hydrogen Joint Undertaking) through the European Union's Horizon 2020 Research and Innovation Action project MAMA-MEA – Mass Manufacture of MEAs Using High Speed Deposition Processes (grant agreement no.: 779591). The authors also wish to specifically thank the colleagues at Johnson Matthey Fuel Cells and Nedstack Fuel Cell Technology for supporting this research by supplying materials and performing dedicated measurements.

REFERENCES

[1] Elmer T, Worall M, Wu S, Riffat SB. Fuel cell technology for domestic built environment applications: state of-the-art review. Renew Sustain Energy Rev 2015;42:913–31. https://doi.org/10.1016/j.rser.2014.10.080.

[2] Lü X, Qu Y, Wang Y, Qin C, Liu G. A comprehensive review on hybrid power system for PEMFC-HEV: issues and strategies. Energy Convers Manag 2018;171:1273–91. https://doi.org/10.1016/j.enconman.2018.06.065.

[3] Moreno NG, Molina MC, Gervasio D, Robles JFP. Approaches to polymer electrolyte membrane fuel cells (PEMFCs) and their cost. Renew Sustain Energy Rev 2015;52:897–906. https://doi.org/10.1016/j.rser.2015.07.157.

[4] Shin SJ, Lee JK, Ha HY, Hong SA, Chun HS, Oh IH. Effect of the catalytic ink preparation method on the performance of polymer electrolyte membrane fuel cells. J Power Sources 2002;106(1):146–52. https://doi.org/10.1016/S0378-7753(01)01045-X.

[5] Peighambardoust SJ, Rowshanzamir S, Amjadi M. Review of the proton exchange membranes for fuel cell applications. Int J Hydrogen Energy 2010;35(17):9349–84. https://doi.org/10.1016/j.ijhydene.2010.05.017.

[6] Zheng Y. Monolithic fuel cell and method(U S Jpn Outlook 6,838,203 B2).

[7] Brosseau GM. Additive manufacturing for fuel cell flow fields(U S Jpn Outlook 9,444,108 B2).

[8] Kundu S, Fowler MW, Simon LC, Grot S. Morphological features (defects) in fuel cell membrane electrode assemblies. J Power Sources 2006;157(2):650–6. https://doi.org/10.1016/j.jpowsour.2005.12.027.

[9] Cheng X, Yi B, Han M, Zhang J, Qiao Y, Yu J. Investigation of platinum utilization and morphology in catalyst layer of polymer electrolyte fuel cells. J Power Sources 1999;79(1):75–81. https://doi.org/10.1016/S0378-7753(99)00046-4.

[10] Bodner M, García H, Steenberg T, Terkelsen C, Alfaro S, Avcioglu G, et al. Enabling industrial production of electrodes by use of slot-die coating for HT-PEM fuel cells. Int J Hydrogen Energy 2019;44. https://doi.org/10.1016/j.ijhydene.2018.11.091.

[11] Stähler M, Stähler A, Scheepers F, Carmo M, Stolten D. A completely slot die coated membrane electrode assembly. Int J Hydrogen Energy 2019;44(14):7053–8. https://doi.org/10.1016/j.ijhydene.2019.02.016.

[12] Lin J-C, Lai C-M, Ting F-P, Chyou S-D, Hsueh K-L. Influence of hot-pressing temperature on the performance of PEMFC and catalytic activity. J Appl Electrochem 2009;39. https://doi.org/10.1007/s10800-008-9758-1.

[13] Cold pressing of membrane electrode assemblies for high-temperature PEM fuel cells. In: Share D, Krishnan L, Lesperence D, Walczyk D, Puffer R, editors. Proceedings of the ASME 2010 8th international conference on fuel cell science, engineering and technology. ASME 2010 8th international fuel cell science, engineering and technology conference, vol. 2; 2010.

[14] Steenberg T, Hjuler HA, Terkelsen C, Sánchez MTR, Cleemann LN, Krebs FC. Roll-to-roll coated PBI membranes for high temperature PEM fuel cells. Energy Environ Sci 2012;5(3):6076–80. https://doi.org/10.1039/C2EE02936G.

[15] Suzuki T. (Invited) fuel cell stack technology of Toyota. ECS Meeting Abstracts 2016. https://doi.org/10.1149/ma2016-02/38/2560.

[16] Mauger SA, Neyerlin KC, Yang-Neyerlin AC, More KL, Ulsh M. Gravure coating for roll-to-roll manufacturing of proton-exchange-membrane fuel cell catalyst layers. J Electrochem Soc 2018;165(11):F1012–8. https://doi.org/10.1149/2.0091813jes.

[17] Siegel F, Kohl A, Enns E, Willert A, Deger W, Dziallas H, et al. Adapted gravure printing process for the production of

carbon based electrodes. J Print Media Technol Res 2012;3:141–8.
[18] Park I-S, Li W, Manthiram A. Fabrication of catalyst-coated membrane-electrode assemblies by doctor blade method and their performance in fuel cells. J Power Sources 2010;195:7078–82. https://doi.org/10.1016/j.jpowsour.2010.05.004.
[19] Toudret P, Blachot J-F, Heitzmann M, Jacques P-A. Impact of the cathode layer printing process on the performance of MEA integrating PGM free catalyst. Catalysts 2021;11(6). https://doi.org/10.3390/catal11060669.
[20] Ihm J, Ryu H, Bae J, Choo W, Choi D. High performance of electrode with low Pt loading prepared by simplified direct screen printing process in PEM fuel cells. J Mater Sci 2004;39:4647–9. https://doi.org/10.1023/B:JMSC.0000034162.92123.96.
[21] Taylor AD. Inkjet printing of materials for use in fuel cells. U S Jpn Outlook 2009. 0074956 A1.
[22] Shukla S, Domican K, Karan K, Bhattacharjee S, Secanell M. Analysis of low platinum loading thin polymer electrolyte fuel cell electrodes prepared by inkjet printing. Electrochim Acta 2015;156:289–300. https://doi.org/10.1016/j.electacta.2015.01.028.
[23] Krebs FC. Fabrication and processing of polymer solar cells: a review of printing and coating techniques. Sol Energy Mater Sol Cell 2009;93(4):394–412. https://doi.org/10.1016/j.solmat.2008.10.004.
[24] Hutchings IM, Martin GD. Inkjet technology for digital fabrication. Hoboken, NJ, USA: Wiley; 2012.
[25] Morita N, Khalate A, van Buul A, Wijshoff H. Inkjet printheads. In: Hoath SD, editor. Fundamentals of inkjet printing: the science of inkjet and droplets. Hoboken, NJ, USA: Wiley; 2016.
[26] Du S, Li W, Wu H, Abel Chuang P-Y, Pan M, Sui P-C. Effects of ionomer and dispersion methods on rheological behavior of proton exchange membrane fuel cell catalyst layer ink. Int J Hydrogen Energy 2020;45(53):29430–41. https://doi.org/10.1016/j.ijhydene.2020.07.241.
[27] Hutchings IM, Martin GD. Inkjet technology for digital fabrication: fundamentals of inkjet technology. Chichester: John Wiley & Sons, Ltd; Wiley; 2012. 2013.
[28] Park J, Yim S-D, Kim T, Park S, Yoon Y-G, Park G-G, et al. Understanding the mechanism of membrane electrode assembly degradation by carbon corrosion by analyzing the microstructural changes in the cathode catalyst layers and polarization losses in proton exchange membrane fuel cell. Electrochim Acta 2012;83:294–304. https://doi.org/10.1016/j.electacta.2012.07.117.
[29] Mauger SA, Neyerlin KC, Alia SM, Ngo C, Babu SK, Hurst KE, et al. Fuel cell performance implications of membrane electrode assembly fabrication with platinum-nickel nanowire catalysts. J Electrochem Soc 2018;165(3):F238–45. https://doi.org/10.1149/2.1061803jes.
[30] Cheng X, Shi Z, Glass N, Zhang L, Zhang J, Song D, et al. A review of PEM hydrogen fuel cell contamination: impacts, mechanisms, and mitigation. J Power Sources 2007;165. https://doi.org/10.1016/j.powsour.2006.12.012.
[31] Pozio A, Silva RF, Francesco M de, Giorgi L. Nafion degradation in PEFCs from end plate iron contamination. Electrochim Acta 2003;48:1543–9. https://doi.org/10.1016/S0013-4686(03)00026-4.
[32] Taylor AD, Kim EY, Humes VP, Kizuka J, Thompson LT. Inkjet printing of carbon supported platinum 3-D catalyst layers for use in fuel cells. J Power Sources 2007;171(1):101–6. https://doi.org/10.1016/j.jpowsour.2007.01.024.
[33] Shukla S, Stanier D, Saha MS, Stumper J, Secanell M. Analysis of inkjet printed PEFC electrodes with varying platinum loading. J Electrochem Soc 2016;163(7):F677–87. https://doi.org/10.1149/2.1111607jes.
[34] Shukla S. Experimental analysis of inkjet printed polymer Electrolyte fuel cell electrodes [doctor of philosophy]. University of Alberta; 2016.
[35] Malevich D, Saha MS, Halliop E, Peppley BA, Pharoah JG, Karan K. Performance characteristics of PEFCs with patterned electrodes prepared by piezo-electric printing. ECS Trans 2013;50(2):423–7. https://doi.org/10.1149/05002.0423ecst.
[36] Ye L, Gao Y, Zhu S, Zheng J, Li P, Zheng JP. A Pt content and pore structure gradient distributed catalyst layer to improve the PEMFC performance. Int J Hydrogen Energy 2017;42(10):7241–5. https://doi.org/10.1016/j.ijhydene.2016.11.002.
[37] Towne S, Viswanathan V, Holbery J, Rieke P. Fabrication of polymer electrolyte membrane fuel cell MEAs utilizing inkjet print technology. J Power Sources 2007;171(2):575–84. https://doi.org/10.1016/j.jpowsour.2007.07.017.
[38] Hakola L, Parra Puerto A, Vaari A, Maaninen T, Kucernak A, Viik S, et al. Anode ink formulation for a fully printed flexible fuel cell stack. Flex Print Electron 2020;5(2):25002. https://doi.org/10.1088/2058-8585/ab7e16.
[39] Breitwieser M, Klingele M, Britton B, Holdcroft S, Zengerle R, Thiele S. Improved Pt-utilization efficiency of low Pt-loading PEM fuel cell electrodes using direct membrane deposition. Electrochem Commun 2015;60:168–71. https://doi.org/10.1016/j.elecom.2015.09.006.
[40] Breitwieser M, Klose C, Klingele M, Hartmann A, Erben J, Cho H, et al. Simple fabrication of 12 μm thin nanocomposite fuel cell membranes by direct electrospinning and printing. J Power Sources 2017;337:137–44. https://doi.org/10.1016/j.jpowsour.2016.10.094.
[41] Vierrath S, Breitwieser M, Klingele M, Britton B, Holdcroft S, Zengerle R, et al. The reasons for the high power density of fuel cells fabricated with directly deposited membranes. J Power Sources 2016;326:170–5. https://doi.org/10.1016/j.jpowsour.2016.06.132.
[42] Wang Z, Nagao Y. Effects of Nafion impregnation using inkjet printing for membrane electrode assemblies in polymer electrolyte membrane fuel cells. Electrochim Acta 2014;129:343–7. https://doi.org/10.1016/j.electacta.2014.02.133.
[43] Barbir F. PEM fuel cells - theory and practice. Amsterdam, The Netherlands: Elsevier; 2012.
[44] Cannio M, Righi S, Santangelo PE, Romagnoli M, Pedicini R, Carbone A, et al. Smart catalyst deposition by 3D printing for polymer electrolyte membrane fuel cell manufacturing. Renew Energy 2021;163:414–22. https://doi.org/10.1016/j.renene.2020.08.064.
[45] Breitwieser M, Bayer T, Büchler A, Zengerle R, Lyth SM, Thiele S. A fully spray-coated fuel cell membrane electrode assembly using Aquivion ionomer with a graphene oxide/cerium oxide interlayer. J Power Sources 2017;351:145–50. https://doi.org/10.1016/j.jpowsour.2017.03.085.
[46] van Osch THJ, Perelaer J, de Laat AWM, Schubert US. Inkjet printing of narrow conductive tracks on untreated polymeric substrates. Adv Mater 2008;20(2):343–5. https://doi.org/10.1002/adma.200701876.
[47] Zhang Z, Zhu W. Controllable synthesis and sintering of silver nanoparticles for inkjet-printed flexible electronics. J Alloys Compd 2015;649:687–93. https://doi.org/10.1016/j.jallcom.2015.07.195.
[48] Litster S, McLean G. PEM fuel cell electrodes. J Power Sources 2004;130(1):61–76. https://doi.org/10.1016/j.jpowsour.2003.12.055.

[49] Hoath SD. Fundamentals of inkjet printing: the science of inkjet and droplets. Hoboken, NJ, USA: Wiley; 2016.
[50] Santangelo PE, Romagnoli M, Puglia M. An experimental approach to evaluate drying kinetics and foam formation in inks for inkjet printing of fuel-cell layers. Exp Therm Fluid Sci 2022;135:110631. https://doi.org/10.1016/j.expthermflusci.2022.110631.
[51] Lee A, Sudau K, Ahn KH, Lee SJ, Willenbacher N. Optimization of experimental parameters to suppress nozzle clogging in inkjet printing. Ind Eng Chem Res 2012;51(40):13195–204. https://doi.org/10.1021/ie301403g.
[52] Ostergren DG, Zabiak DM. Jet printing ink composition(U S Jpn Outlook 3,846,141).
[53] Liker S. Methods and apparatus for preventing clogging in ink jet printers(U S Jpn Outlook vol. 5,329,293 A).
[54] ASTM. Standard terminology for additive manufacturing technologies. West Conshohocken, PA, USA: ASTM International; 2012. ASTM F2792-12.
[55] Christodoulou KN, Lightfoot EJ, Powell RW. Model of stress-induced defect formation in drying polymer films. AICHE J 1998;44(7):1484–98. https://doi.org/10.1002/aic.690440703.
[56] Marr C, Li X. Composition and performance modelling of catalyst layer in a proton exchange membrane fuel cell. J Power Sources 1999;77(1):17–27. https://doi.org/10.1016/S0378-7753(98)00161-X.
[57] Derby B. Inkjet printing ceramics: from drops to solid. J Eur Ceram Soc 2011;31(14):2543–50. https://doi.org/10.1016/j.jeurceramsoc.2011.01.016.
[58] Wieser C. Novel polymer electrolyte membranes for automotive applications - requirements and benefits. Fuel Cell 2004;4(4):245–50. https://doi.org/10.1002/fuce.200400038.
[59] Cho J, Kim H-S, Min K. Transient response of a unit proton-exchange membrane fuel cell under various operating conditions. J Power Sources 2008;185(1):118–28. https://doi.org/10.1016/j.jpowsour.2008.06.073.
[60] Kienitz B. Optimizing polymer electrolyte membrane thickness to maximize fuel cell vehicle range. Int J Hydrogen Energy 2021;46(19):11176–82. https://doi.org/10.1016/j.ijhydene.2020.03.126.
[61] Balzarotti R, Latorrata S, Stampino P, Cristiani C, Dotelli G. Development and characterization of non-conventional micro-porous layers for PEM fuel cells. Energies 2015;8(7):7070–83. https://doi.org/10.3390/en8077070.
[62] Balzarotti R, Latorrata S, Mariani M, Gallo Stampino P, Dotelli G. Optimization of perfluoropolyether-based gas diffusion media preparation for PEM fuel cells. Energies 2020;13(7):1831. https://doi.org/10.3390/en13071831.
[63] Larbi B, Alimi W, Chouikh R, Guizani A. Effect of porosity and pressure on the PEM fuel cell performance. Int J Hydrogen Energy 2013;38(20):8542–9. https://doi.org/10.1016/j.ijhydene.2012.11.022.
[64] Lü W, Liu Z, Wang C, Mao Z, Zhang M. The effects of pinholes on proton exchange membrane fuel cell performance. Int J Energy Res 2011;35(1):24–30. https://doi.org/10.1002/er.1728.